Int. J. Environ. Sci. Technol. (2018) 15:2283–2294
https://doi.org/10.1007/s13762-017-1624-4

ORIGINAL PAPER

Kinetic and equilibrium studies on the removal of ^{14}C-ethion residues from wastewater by copper-based metal–organic framework

R. M. Abdelhameed[1] · H. Abdel-Gawad[1] · C. M. Silva[2] · J. Rocha[2] · B. Hegazi[1] · A. M. S. Silva[3]

Received: 15 June 2017 / Revised: 9 October 2017 / Accepted: 19 October 2017 / Published online: 31 October 2017

Abstract There are compelling economic and environmental reasons to remove pesticides from wastewater because they are toxic and carcinogenic. The effectiveness of copper-based metal–organic framework (Cu-BTC) for adsorbing the insecticide ^{14}C-ethion from wastewater has been studied as function of contact time, adsorbent dosage, temperature and pH. ^{14}C-ethion/Cu-BTC isotherms exhibit two plateaus (BET type IV) and are reliably represented by Brunauer–Deming–Deming–Teller and Zhu–Gu models, with deviations of only 1.99 and 3.95%, respectively. The removal curve measured under batch operation is well represented by a pseudo-first-order equation, yielding results equivalent to the theoretical linear driving force model of Glueckauf. At pH 7, 75 mg L^{-1} ethion concentration, 150 min, 25 °C and 0.425 g L^{-1} Cu-BTC dose, the sorbent capacity is ca. 122 mg g^{-1}. Moreover, Cu-BTC has a good stability after six adsorptions cycles. Finally, our results disclose the fundamental understanding of the adsorption mechanism: the ethion molecule coordinates to two copper(II) atoms across the metal–organic framework channel via the phosphoryl (P–O) group.

Keywords Adsorption mechanism · Copper-based metal–organic framework · Ethion · Kinetics · Modeling · Type IV isotherm

Introduction

Searching for clean fresh water sources has become an important issue at the local and global levels because water is an essential resource for humans and, indeed, all living organisms. In Egypt, the key problem of water resources is the imbalance between the increasing demand and limited supply. Another outstanding issue is the poor quality of the wastewater, which is often contaminated with high amounts of toxic organic compounds, such as herbicides, insecticides, fungicides and bactericides, constituting a major challenge for its reuse (Qadir et al. 2015). These pesticides encompass organophosphorus, organochlorine, carbamates, anilines, ureas and pyrethroids. Organophosphorus pesticides are the most widely used, amounting to several billion US dollars annually, including the insecticide ethion (*O*,*O*,*O*′,*O*′-tetraethyl-*S*,*S*′-methylene-bisphosphorodithioate) (Abdel-Gawad et al. 2011). The residues of organophosphorus pesticides reach the agriculture wastewaters due to failed spray over crops and soils. The presence of pesticide residues in all types of water is a public health concern, and thus, it is very important to develop novel technologies for their removal. The European Environment Agency stipulates a maximum residue level (MRL) for pesticides in drinking water of 0.1 μg L^{-1}. According to a report on the surveillance of pesticide in water in Egypt (Initiative \), there is a significant concentration (0.4–1.0 mg L^{-1}) of ethion residues in water samples. Moreover, ethion reaches a high concentration in dip

Editorial responsibility: V.K. Gupta.

✉ A. M. S. Silva
artur.silva@ua.pt

[1] Applied Organic Chemistry Department, National Research Centre, 33 EL Bohouth st., Dokki, Giza, Egypt

[2] Department of Chemistry, CICECO, University of Aveiro, 3810-193 Aveiro, Portugal

[3] Department of Chemistry, QOPNA, University of Aveiro, 3810-193 Aveiro, Portugal

sludges and surrounding soils (up to 45 g kg^{-1}) (Foster et al. 2004).

The methods available for pesticides removal from water include advanced oxidation processes, aerobic degradation, photocatalytic degradation, combined photo-Fenton, biological oxidation, nanofiltration, ozonation and adsorption (Ahmad et al. 2010). The adsorption process is widely used for water treatment and removal of organic pollutants from wastewater, being simple in terms of design and operation (Saleh et al. 2017; Danmaliki et al. 2017; Danmaliki and Saleh 2017). Much work is available on the development of materials for adsorption of organic and inorganic pollutants from industrial wastewaters, including forestry and agricultural residues, and by-products as low-cost adsorbents. Although activated carbon is a powerful adsorbent in water and wastewater treatment, it is relatively expensive and its recycling is not efficient (Ahmad et al. 2010).

An excellent sorbent should exhibit both high capacity and good transport properties, which rely on appropriate functional groups, large specific surface area and favorable pore size distribution. Unfortunately, most of the current inorganic sorbents rarely combine such features simultaneously; for example, carbon nanotubes have high surface area, but no suitable functional groups. In contrast, the organic polymer polyphenylenediamine has a large number of amino and imino groups, but a small specific area and slow adsorption kinetics limit its application (Huang et al. 2006). Metal oxide composites exhibit many advantages, such as excellent efficiency for degrading various pollutants (photocatalytic treatment), cost effectiveness, low risk to the environment and high stability (Gupta et al. 2017; Saravanan et al. 2016). ZnS:Cu nanoparticles supported on activated carbon were used to remove auramine-*O* from aqueous solutions with an adsorption capacity of 183.15 mg g^{-1} (Asfaram et al. 2015). 2-Hydroxyethyl methacrylate, 2-hydroxyethyl methacrylate–ethoxy ethyl methacrylate–methacrylic acid and poly(vinyl alcohol) were used to uptake malachite green and Congo red from aqueous solutions. The adsorption affinity of Congo red onto poly(vinyl alcohol) was 169–236 mg g^{-1}, for 2-hydroxyethyl methacrylate–ethoxy ethyl methacrylate–methacrylic acid 90–155 mg g^{-1} and for 2-hydroxyethyl methacrylate 17–57 mg g^{-1}. The maximum adsorption of malachite green onto 2-hydroxyethylmethacrylate was 130–205 mg g^{-1} and for poly(vinyl alcohol) 35–140 mg g^{-1} (Gupta et al. 2015). Graphene oxide was also used to remove basic red 12 and methyl orange from aqueous solutions, with capacities of 63.69 and 16.83 mg g^{-1}, respectively (Robati et al. 2016).

Metal–organic frameworks (MOFs) are a class of microporous organic–inorganic hybrid materials (Li et al. 1999), which have received much attention in the last years due to both their unique structures built up from self-assembling metal ions and multifunctional organic ligands, and their promising applications in gas storage, separation processes, drug delivery, fuel purification and catalysis (Abdelhameed et al. 2017; Stavila et al. 2014; Zhang and Lin 2014), among others. In the context of this article, MOFs are important materials because they present high adsorption capacity and favorable kinetics. Only a few studies are available on the use of MOFs on the adsorptive removal of organophosphorus pesticides from aqueous solutions (Zhu et al. 2014).

Copper-based *MOF denoted* Cu-BTC (also known as HKUST-1) has chemical formula $Cu_3(BTC)_2$ [BTC = 1,3,5-benzenetricarboxylate] and a copper oxide (CuO) backbone structure. The importance of CuO lays on its nontoxicity, its constituents are commercially available, and this type of structure was already applied in catalysts, sensors, electronic and optoelectronic devices, solar cells and degradation of textile dyes. In our previous work (Abdelhameed et al. 2016), we designed a composite of Cu–BTC and cotton fabric, very active in the removal of ethion insecticide from water. The adsorption equilibrium data were reliably fitted by the Langmuir model. Consequently, we decided to study the effect of Cu–BTC MOF alone on the removal of the organophosphorus insecticide ^{14}C-ethion from wastewater. After the synthesis and characterization of Cu-BTC, equilibrium and kinetic experiments were performed under different operating conditions (sorbent dose, pH and temperature), followed by their rigorous modeling and analysis. All the tests were performed at the National Research Centre, Egypt, from May to September 2015.

Materials and methods

Synthesis of Cu-BTC

Cu-BTC MOF was synthesized according to the literature (Rowsell and Yaghi 2006; Liu et al. 2007). Copper(II) nitrate trihydrate (2.077 g) was dissolved in water (15 mL) and added to a solution of 1,3,5-benzenetricarboxylic acid (1.0 g) in a 1:1 mixture of ethanol/*N*,*N*-dimethylformamide (DMF) (30 mL) and stirred for 10 min. The resulting solution was then transferred into a Teflon-lined stainless steel autoclave and heated at about 100 °C for 10 h. The reaction vessel was cooled to room temperature, and the resulting blue crystals were isolated by filtration and Soxhlet extracted with methanol overnight to remove DMF. The product was then dried at room temperature.

Synthesis of ^{14}C-ethion

^{14}C-ethion labeled at the second carbon atom of the ethyl group **2** was prepared in a single vessel reaction using ^{14}C-

ethanol (Sp. Act. 37 MBq, Amersham, England), methylene chloride and *O,O*-diethyl hydrogen phosphorodithioate according to previous work (Abdel-Gawad et al. 2011). Briefly, the method is (Scheme 1): 10 g of P_2S_5 was dissolved in 40 mL benzene at 40 °C (mixture I). Labeled ^{14}C-ethanol (12 mL, Sp. Act 37 MBq) was added dropwise to mixture I and stirred for 3 h producing compound **1**. A solution of methylene chloride (3.5 mL) and triethylamine (13.5 mL) in benzene (20 mL) was added dropwise to **1**. The reaction mixture was stirred at 25 °C for 20 min and then refluxed for 3 h. The resulting mixture was filtered to remove triethylamine hydrochloride and evaporated under vacuum to remove the solvent. The prepared ^{14}C-ethion (**2**) had a specific activity of 7.4 MBq g^{-1} and 98% radiometric purity.

Characterization of the materials

The morphology of the synthesized product was characterized by scanning electron microscopy (SEM Quanta FEG 250 with field emission gun, FEI Company—Netherlands), and the chemical composition of the samples was determined by energy dispersive X-ray spectroscopy (EDS) (EDAX AMETEK analyzer) coupled to the electron microscope. The samples were also characterized by powder X-ray diffraction (XRD) on a Philips X'Pert MPD diffractometer with graphite monochromatized Cu Kα radiation ($\lambda = 1.5406$ Å) in the 2θ range 3.5°–50°, with a step size of 0.05° and scanning rate 1 s per step. Fourier transform infrared (FTIR) spectra were collected on a Mattson 5000 spectrometer in the range 4000–350 cm^{-1} in transmission mode using KBr pellets compressed at 10 kPa.

Insecticide analysis

Radioactivity assay method was used to detect and quantify ^{14}C-ethion. Radioactivity of solution samples from the various adsorption experiments was determined using a Packard liquid scintillation spectrometer (Model TRI-CARB 2300 TR) in vials containing a 1,4-dioxane-based scintillation cocktail. Radioactivity levels were all corrected for quenching using an internal standard.

Adsorption experiments

^{14}C-ethion (75 ppm) stock solution was prepared by dissolving ^{14}C-ethion in a small amount of acetone (2 mL) and deionized water. The adsorption experiments were carried out under batch conditions and comprised stirring 200 mL of this solution with 5–100 mg Cu-BTC, for 15–180 min, pH 6, 7 and 8, and temperature 25, 35 and 45 °C. Adsorbent particles were separated out from the liquid by centrifugation at 5000 rpm for 10 min. Efficiency of ^{14}C-ethion removal from the aqueous solutions was calculated by:

$$R\,(\%) = 100\,\frac{C_0 - C_t}{C_0} \tag{1}$$

where C_0 is the initial concentration of insecticide and C_t is the concentration at any time t. All experiments were carried out in triplicate, and the results are the mean of these independent measurements.

The average concentration of ^{14}C-ethion in the MOFs at any time t (q_t, mg g^{-1}) was calculated as function of C_t by trivial material balance to the adsorber:

$$q_t = \frac{V_L}{m_{ads}}\,(C_0 - C_t) \tag{2}$$

where V_L is the solution volume (L) and m_{ads} is the adsorbent mass (g); Eq. 2 is the well-known operating line of the separation system. At long times, mathematically $t = \infty$, the system reaches equilibrium and the two concentrations—hereafter denoted by (C_e, q_e)—represent one point of the ^{14}C-ethion/Cu-BTC isotherm.

Kinetic study

Adsorption kinetics of ^{14}C-ethion onto Cu-BTC was modeled using pseudo-first-order (or Lagergreen) (Largergren 1898) and pseudo-second-order (Ho and McKay 1999) equations, whose linearized forms are given by Eqs. 3 and 4, respectively:

$$\ln(q_e - q_t) = \ln q_e - k_1 t \tag{3}$$

$$\frac{t}{q_t} = \frac{1}{k_2 q_e^2} + \frac{1}{q_e}\,t \tag{4}$$

where q_t (mg g^{-1}) is the solid loading at time t (min), q_e is the concentration at equilibrium (i.e., for $t = \infty$),

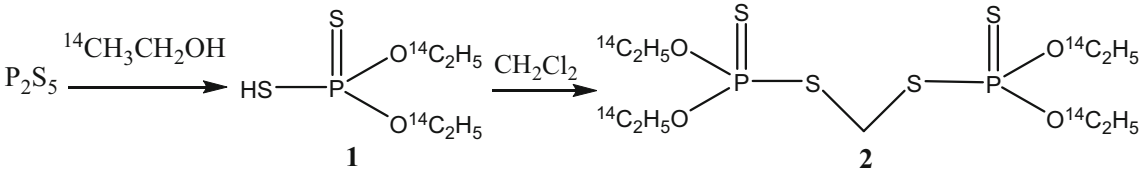

Scheme 1 Synthesis of ^{14}C-ethion

$k_1(\text{min}^{-1})$ is the rate constant of the pseudo-first-order equation and k_2 (g mg^{-1} min^{-1}) is the rate constant of the pseudo-second-order equation.

Adsorption isotherms

The relation between the adsorbate concentrations in solution and solid phases at constant temperature is the system isotherm, which in the case of ^{14}C-ethion/Cu-BTC can be classified as type IV (see "Adsorption isotherms"), since it combines the favorable BET mechanism with an upper limiting plateau at higher concentrations (Brunauer et al. 1940; Do 1998). Such two plateau-type isotherms detach from the majority found in the literature.

Brunauer et al. (1940) developed a theory able to describe type IV (and type V) isotherms, which will be henceforth named Brunauer–Deming–Deming–Teller. For liquid solutions, it can be expressed as:

$$q_e = q_m \frac{Zx}{1-x} \frac{1+(ng/2-n)x^{n-1}-(ng-n+1)x^n+(ng/2)x^{n+1}}{1+(Z-1)x+(Zg/2-Z)x^n-(Zg/2)x^{n+1}}, \quad \text{with } x = C_e/C_s \tag{5}$$

where q_m is the monolayer adsorption capacity, C_s may be taken as equivalent to the maximum solution concentration (i.e., solubility) and Z, n and g are additional adjustable parameters. Parameter g is related to the extra adsorption energy observed at higher solute layers and depends on temperature. In this work, the following dependency was adopted for $g(T)$:

$$\ln g = a_{BET}T + b_{BET} \tag{6}$$

where a_{BET} and b_{BET} are fitting coefficients. In this way, two parameters are embodied in spite of one g per temperature.

An alternative approach to represent the equilibrium data of ^{14}C-ethion/Cu-BTC system relies on the work of Zhu and Gu (1989) who has derived a general isotherm for the adsorption of surfactants based on a two-step mechanism and mass action law. The first step corresponds to the solute adsorption onto the pore walls, while the second represents the interaction between free and adsorbed molecules. Isotherm equation is given by:

$$q_e = q_{max} \frac{K_1 C_e \left(\frac{1}{n} + K_2 C_e^{n-1}\right)}{1 + K_1 C_e \left(1 + K_2 C_e^{n-1}\right)} \tag{7}$$

where q_{max} is the limiting/maximum adsorption at high concentration (i.e., solid capacity), K_1 and K_2 are the equilibrium constants of the aforementioned first and second steps, respectively, and n is an aggregation number. Under the experimental conditions of this work, K_1 is essentially constant, while an exponential temperature dependency was assumed for K_2:

$$\ln K_2 = a_{Zhu}T + b_{Zhu} \tag{8}$$

Equation 7 is able to reproduce not only *Langmurian* trends, but also isotherms with two plateaus (e.g., type IV), being inclusively used in other systems than surfactants (Zhu et al. 1989; Girods et al. 2009; Hoffmann et al. 2012). A limitation of this model is that its parameters are heavily correlated (Sainio and Turku 2010), and thus, care must be taken during optimization.

Isotherm parameters were obtained through unconstrained nonlinear regression using the Nelder–Mead algorithm, minimizing the residual sum of squares (*RSS*) as objective function:

$$\text{RSS} = \sum_{i=1}^{\text{NDP}} \left(q_{\text{calc},i} - q_{\text{exp},i}\right)^2 \tag{9}$$

Here, $q_{\text{calc,i}}$ and $q_{\text{exp,i}}$ are the calculated and experimental concentrations in the solid phase, respectively, and NDP is the number of data points. The quality of the fitting is expressed by the average absolute relative deviation, AARD:

$$\text{AARD}\,(\%) = \frac{100}{\text{NDP}} \sum_{i=1}^{\text{NDP}} \frac{\left|q_{\text{calc},i} - q_{\text{exp},i}\right|}{q_{\text{exp},i}} \tag{10}$$

All models and programs developed in this work were coded in MATLAB R2009a®.

Results and discussion

Materials characterization

Figure 1 shows the powder XRD patterns of Cu-BTC and ^{14}C-ethion insecticide adsorbed on Cu-BTC. Main diffraction peaks of both materials are the same, indicating that the crystalline structure is preserved upon ^{14}C-ethion adsorption. All samples exhibit reflections at 6.8, 9.6, 11.8 and 13.5 assigned to, respectively, (200), (220), (222) and (400) Cu–BTC crystal planes. SEM images of Cu-BTC before and after ^{14}C-ethion adsorption are shown in Fig. 2. Cu-BTC shows crystals with size in the range 3–10 μm (Fig. 2a, c). After ^{14}C-ethion adsorption, smaller Cu-BTC crystals are observed (Fig. 2b). Figure 3 compares the FTIR spectra of ^{14}C-ethion, Cu-BTC and ^{14}C-ethion adsorbed on Cu-BTC. ^{14}C-ethion gives absorption peaks at 2980, 2936 and 2901 cm^{-1} (not shown) ascribed to aliphatic C-Hs. Sharp peak at 1016 cm^{-1} is assigned to PO-Et and a band at 960 cm^{-1} to POC-C. Bands at 816/796, 651 and 505 cm^{-1} are assigned to P-OEt, P = S and P–S,

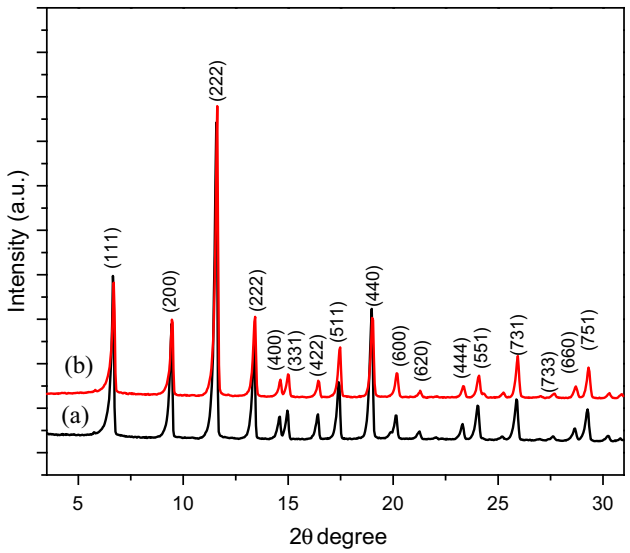

Fig. 1 Powder XRD patterns of **a** as-synthesized Cu-BTC and **b** ^{14}C-ethion adsorbed on Cu-BTC

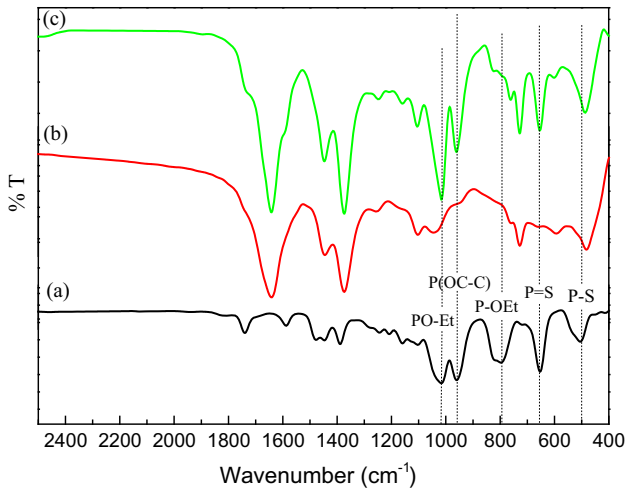

Fig. 3 FTIR spectra of **a** ^{14}C-ethion insecticide, **b** Cu-BTC and **c** ^{14}C-ethion adsorbed on Cu-BTC

respectively (Fig. 3a) (Tanner and Leung 1996). In Fig. 3b, the bands at ca. 1636, 1452 cm^{-1} assigned to the carboxylate ligands witness the BTC coordination to copper. Band at 1111 cm^{-1} is assigned to the C–O–Cu stretching of Cu-BTC. Bands at 760 and 730 cm^{-1} are attributed to vibrational modes of the Cu species (Vishnyakov et al. 2003). The spectrum of ^{14}C-ethion adsorbed on Cu-BTC (Fig. 3c) exhibits the characteristic bands of ^{14}C-ethion at 2980 (aliphatic C-Hs), 1016 (PO-Et), 960 (POC-C) and 651 (P = S) cm^{-1}. Importantly, the ^{4}C-ethion P-OEt (Tanner and Leung 1996) bands at 816 and 796 cm^{-1} disappear upon pesticide adsorption, indicating that this molecule coordinates to Cu(II) via the phosphoryl group (P–O).

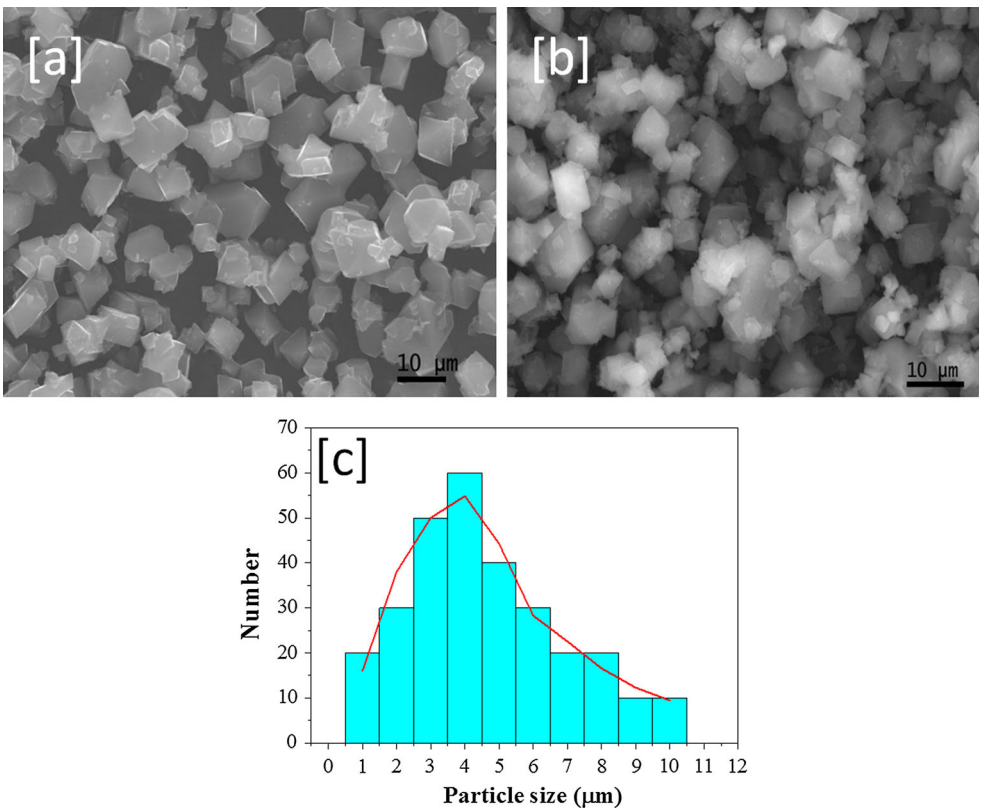

Fig. 2 SEM images of **a** as-synthesized Cu-BTC, **b** ^{14}C-ethion adsorbed on Cu-BTC and **c** Cu-BTC particle size distribution

Study of ^{14}C-ethion removal by Cu-BTC

Effect of the amount of Cu-BTC

Figure 4 shows the removal percentage of ^{14}C-ethion (200 mL solution of 75 ppm) after 150 min using different amounts (5–100 mg) of Cu-BTC at 25, 35 and 45 °C, at pH 7. Removal increases from 18.6 to 100% when the dosage of Cu-BTC increases from 5 mg/200 mL to 100 mg/200 mL, respectively. The ^{14}C-ethion uptake versus Cu-BTC dose shows a slight decrease as temperature is raised from 25 to 45 °C. Furthermore, the removal increases with increasing adsorbent dose since the number of active sorption sites is proportional to the mass of solid. Accordingly, the highest removal efficiency was attained for the maximum Cu-BTC dose of 100 mg/200 mL. The value of 85 mg/200 mL was chosen as a good dose compromise for further experiments.

Effect of contact time and temperature

Effect of contact time (15–180 min) on the removal of ^{14}C-ethion from aqueous solution was determined at different temperatures (25, 35, 45 °C) and pH values (6, 7, 8) as shown in Fig. 5. In all cases, 85 mg of Cu-BTC and 200 mL solution with the initial concentration 75 ppm have been used. As Fig. 5 illustrates, the adsorption of ^{14}C-ethion increases with time and tends to a plateau when the equilibrium is achieved. In all cases, the initial adsorption rate is faster due to the large mass transfer driving forces that prevail when Cu-BTC is essentially clean. The highest percentage (95%) of ^{14}C-ethion uptake onto Cu-BTC is attained at pH 7 and 25 °C after 90 min, when equilibrium is almost reached.

Concerning the influence of temperature on ^{14}C-ethion adsorption, Fig. 5 shows the removal percentage changed from 77 to 54 (pH 6), 95 to 82 (pH 7) and 87 to 73 (pH 8) as the temperature increased from 25 to 45 °C. Removal of ^{14}C-ethion is strongly dependent on temperature, with the highest adsorption always reached at 25 °C after long contact times, i.e., near equilibrium, showing the exothermic nature of the process.

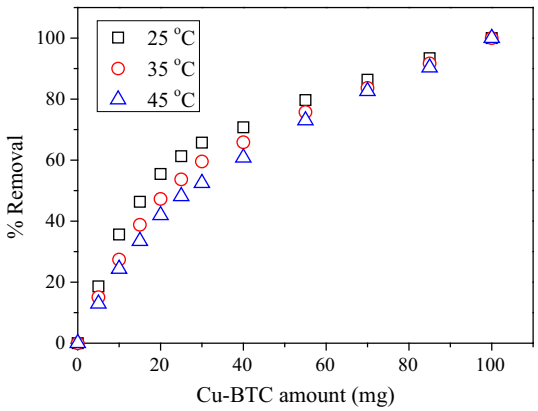

Fig. 4 Effect of adsorbent (Cu-BTC) dose on the removal of ^{14}C-ethion from aqueous solution. Exp. conditions: $V_L = 200$ mL, $C_0 = 75$ ppm, pH 7

Effect of pH

pH is a very important factor influencing the adsorption of ^{14}C-ethion, and it was studied in the range 6–8 with the objective to simulate wastewater media. Insecticide removal increases in the order pH 7 > 8 > 6 (Fig. 5). pH 7 was assumed to be the optimum value for ^{14}C-ethion/Cu-BTC system, and thus, all subsequent equilibrium and kinetic experiments were run at this pH.

Adsorption isotherms

^{14}C-ethion/Cu-BTC isotherms measured at three different temperatures are plotted in Fig. 6. The experimental results confirm the solid loading obeys the expected trend $q_e(25\ °C) > q_e(25\ °C) > q_e(25\ °C)$, since adsorption is an exothermic process. Concerning the behavior of the equilibrium data, Fig. 6 shows that the present system is of type IV, taking into account the first plateau and the limiting maximum disclosed at high concentrations. It is also worth noting that the form of q_e approaches a step function very near the origin, meaning that the three isotherms are approximately irreversible in this region. This is a very unusual, but favorable behavior. ^{4}C-ethion/Cu-BTC equilibrium was modeled using Brunauer–Deming–Deming–Teller (Eqs. 5 + 6) and Zhu–Gu (Eqs. 7 + 8) isotherms. The calculated results are graphically displayed in Fig. 6, and the optimized parameters and average errors are listed in Table 1. In both cases, excellent results were achieved, considering the low deviations found (AARD = 1.99 and 3.95%, respectively) simultaneously for three curves (25, 35 and 45 °C) with abnormal steepest behavior near origin. Zhu–Gu isotherm over estimates the adsorbed concentration associated with the first equilibrium (i.e., first plateau), but performs reliably for $C_e \geq 1$ mg L^{-1}. Large K_1 value (Table 1: $K_1 = 7.21 \times 10^6$ L mg^{-1}) was expected since it corresponds to the equilibrium constant of the first adsorption step (Zhu and Gu 1989), which is essentially irreversible. Moreover, a single K_1 was fitted to the data because the first equilibrium is the same for the three temperatures. Nonetheless, the isotherm splits then into three distinct curves, one for each temperature, which implies K_2 is temperature dependent, as Eq. 8 demonstrates. Calculated $K_2(T)$ is 7.68×10^{-3}, 3.22×10^{-3} and 1.35×10^{-3}mg^{1-n}L^{n-1} for 25, 35 and 45 °C, respectively, which are theoretically consistent parameters since the

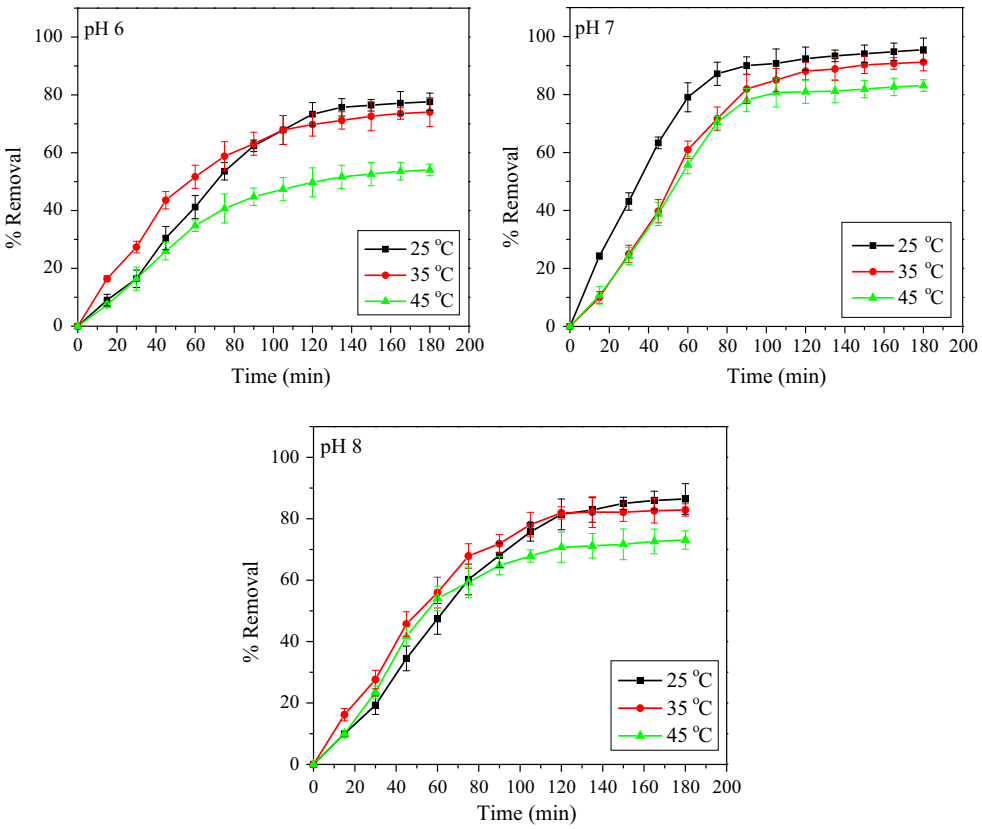

Fig. 5 Effect of contact time on ^{14}C-ethion removal by Cu-BTC. Exp. conditions: $V_L = 200$ mL, $m_{ads} = 85$ mg, $C_0 = 75$ ppm. Curves: lines to guide the eyes; symbols: data points

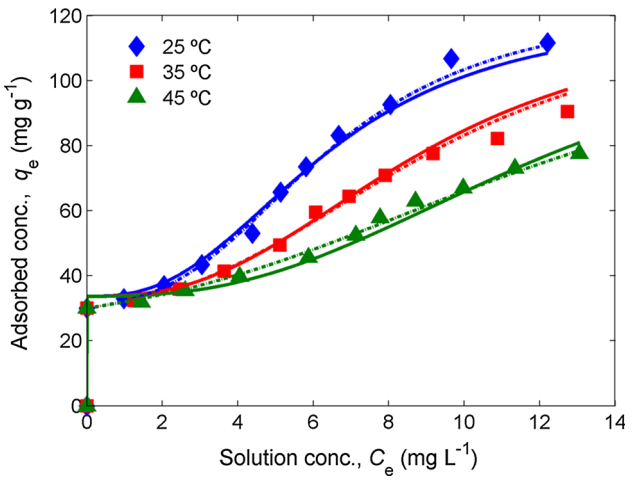

Fig. 6 Equilibrium isotherms of ^{14}C-ethion/Cu-BTC system at pH 7.0. Symbols: data points; solid line, model of Zhu–Gu (Zhu and Gu 1989); dashed line, type IV isotherm of Brunauer–Deming–Deming–Teller (Brunauer et al. 1940; Do 1998)

higher the value of K_2, the steeper the second isotherm step (Zhu and Gu 1989) (Fig. 6). Brunauer–Deming–Deming–Teller model (Eqs. 5 + 6) achieved the best fitting results (AARD = 1.99%) and very reliable parameters, as follows. (1) The value of q_m is the monolayer capacity, which corresponds to the value of the first isotherm step; adjusted parameter ($q_m = 30.0$ mg g^{-1}, Table 1) agrees with measured data (Fig. 6). (2) Similarly to parameter K_1 of Zhu–Gu model, the value of Z is very high ($Z = 1.59 \times 10^8$, Table 1) because the larger the value, the sooner the isotherm convexity increases toward the low concentration range; moreover, since $Z \gg 1$, a type IV isotherm results (if $Z < 1$, isotherm would be of type V, instead). (3) Parameter g is linked to the extra adsorption energy and is temperature dependent (Eq. 6). In this work, their values attain 49.9, 16.0 and 5.11 at 25, 35 and 45 °C, respectively, which are theoretically coherent because the higher g, the sooner the second plateau emerges and the curve splitting occurs (Fig. 6). (iv) As a first approximation, C_s can be taken as the solute solubility; however, it has been reported that it should be adjusted to data when BET type isotherms are extended to liquid solutions (Ebadi et al. 2009). In the present case, $C_s = 16.4$ mg L^{-1} is of the same order of magnitude of ^{14}C-ethion solubility. (v) Finally, it is of interest to check the consistency between parameters of both models. The sorbent capacity given by Zhu–Gu isotherm is $q_{max} = 122$ mg g^{-1} (Eqs. 7 + 8 and Table 1). In the BET case (Eqs. 5 + 6), the horizontal asymptote corresponds to the limiting $q_e \rightarrow n \times q_m$, i.e., the maximum solid loading is $q_e = 4.19 \times 30 = 125.7$ mg g^{-1}. Besides the Cu-BTC capacity, it is also significant the vicinity of both n values (3.63 and 4.19, Table 1).

Table 1 Calculated isotherms for the ^{14}C-ethion/Cu-BTC system at 25, 35 and 45 °C and pH 7.0

Model	Parameters	AARD (%)
Brunauer–Deming–Deming–Teller (Eqs. 5 + 6)	$q_m = 30.0$ mg g^{-1} $C_s = 16.4$ mg L^{-1} $Z = 1.59 \times 10^8$ $n = 4.19$ $\ln g = -0.114T\,(\mathrm{K}) + 37.9$	1.99
Zhu–Gu (Eqs. 7 + 8)	$q_{max} = 122$ mg g^{-1} $K_1 = 7.21 \times 10^6$ L mg^{-1} $n = 3.63$ $\ln K_1(\mathrm{mg}^{1-n}\,\mathrm{L}^{n-1}) = -0.0871T\,(\mathrm{K}) + 21.1$	3.95

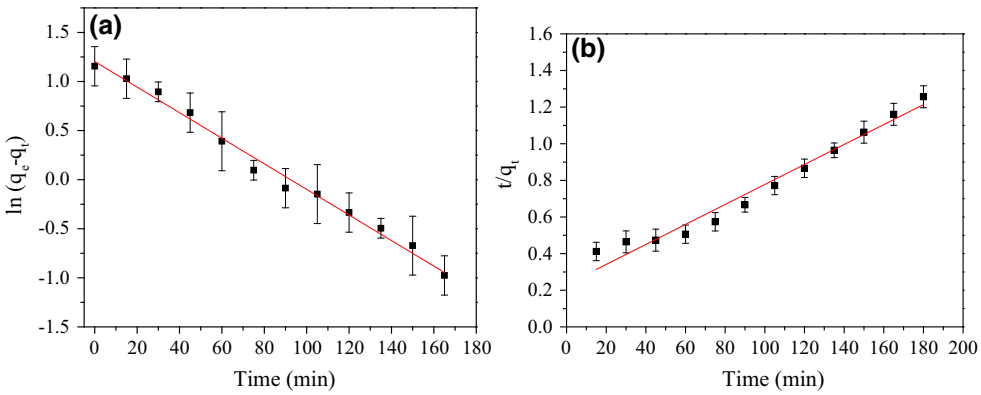

Fig. 7 Linearized **a** pseudo-first-order plot and **b** pseudo-second-order plot for ^{14}C-ethion removal using Cu-BTC. Exp. conditions: $V_L = 200$ mL, $m_{ads} = 85$ mg, $C_0 = 75$ ppm, $T = 25$ °C, pH 7.0. Lines, models; symbols, data points

Adsorption kinetics

Adsorption kinetics depends on the average particle diameter, pore size distribution, adsorbate–adsorbent interactions and operating conditions. The adsorption rate is an important feature determining the selection of the solid, which should exhibit a large capacity and favorable effective diffusivities. Most studies use pseudo-first-order and pseudo-second-order models to represent removal curves. k_1 determined from the slope of the linear plot of $\ln(q_e - q_t)$ against t (Fig. 7a) is 0.0276 min^{-1}. Even if the plot of (t/q_t) against t has a linear bias (Fig. 7b), a rate constant $k_2 = 1.3 \times 10^{-4}$ g mg^{-1} · min^{-1} was determined from the intercept of the approximated linear fitting. Lagergreen or pseudo-first-order model (Largergren 1898) is frequently adopted in adsorption and ion exchange processes due to its simplicity, notwithstanding its empirical nature and lack of predictive ability (Rodrigues and Silva 2016). Its mathematical expression states that the rate of adsorption is proportional to the "distance to the final equilibrium" concentration of the solid $(q_e - q_t)$:

$$\frac{dq_t}{dt} = k_1(q_e - q_t) \tag{11}$$

Alternatively, the linear driving force (LDF) model of Glueckauf describes the intraparticle mass transfer in adsorption processes by the simple, but physically consistent equation (Glueckauf and Coates 1947; Glueckauf 1955; Aniceto and Silva 2015):

$$\frac{dq_t}{dt} = k_{LDF}(q_{e,t} - q_t) \tag{12}$$

where the driving force to mass transport inside the particle is the difference between the adsorbed phase concentration at particle/fluid interface (which is in equilibrium with bulk concentration when the external film is negligible; $q_{e,t}$) and the average concentration in the particle (q_t), i.e., $(q_{e,t} - q_t)$. For *homogeneous* particles, the kinetic constant of the LDF model of Glueckauf is simply $k_{LDF} = 15D_h/R_p^2$ (Glueckauf and Coates 1947; Glueckauf 1955; Aniceto and Silva 2015), where R_p is the particle radius and D_h is the adsorbate diffusivity in the particle. Taking into account Eqs. 11 and 12, it is now possible to explain the good fit achieved by the pseudo-first-order model, which should not be attributed only to empirical correlation. In Fig. 8 are plotted the Brunauer–Deming–Deming–Teller isotherm (Eqs. 5 + 6) at 25 °C and the operating line (Eq. 2), being possible to conclude that over the whole region of operation the isotherm is basically given by its maximum value. Hence, the values of the instantaneous solid loadings in equilibrium with bulk solution, $q_{e,t}$, are equal to the final

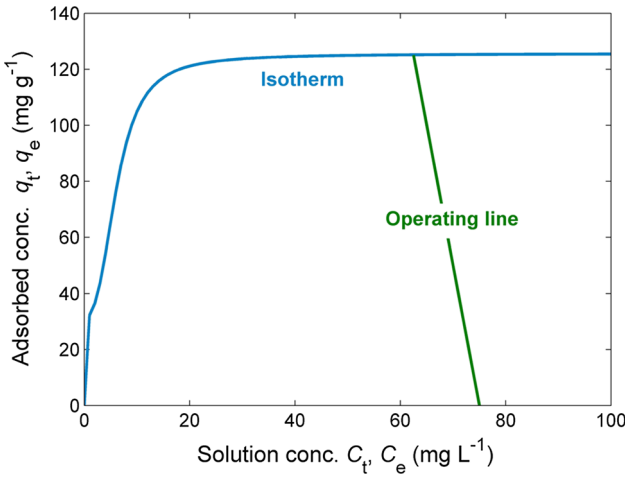

Fig. 8 Brunauer–Deming–Deming–Teller isotherm of ^{14}C-ethion/Cu-BTC system (Eqs. 5 + 6) and material balance to the adsorber (operating line, Eq. 2). Exp. conditions: $V_L = 200$ mL, $m_{ads} = 85$ mg, $C_0 = 75$ ppm, $T = 25$ °C, pH 7.0

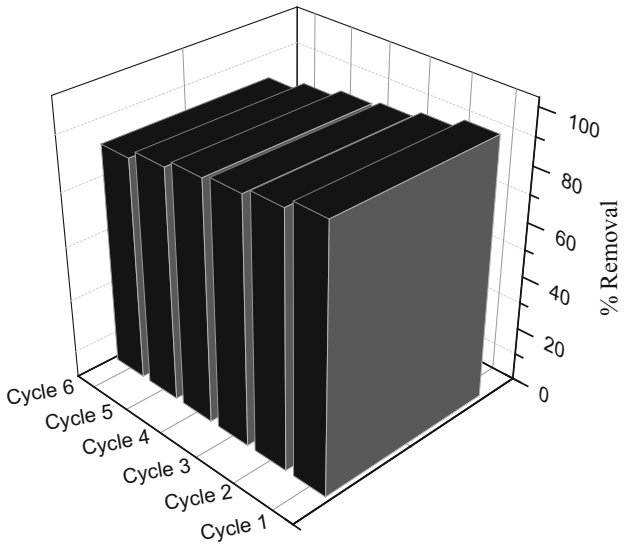

Fig. 9 Regeneration and reuse of Cu-BTC. Exp. conditions: $V_L = 200$ mL, $m_{ads} = 85$ mg, $C_0 = 75$ ppm, $T = 25$ °C, pH 7.0, and contact times of 150 min

equilibrium concentration q_e, which implies that the empirical Lagergreen equation becomes equivalent to the LDF model derived by Glueckauf. In conclusion, the results achieved in this section possess a solid theoretical background.

Reusability of Cu-BTC adsorbent

Besides favorable equilibrium and kinetic properties, a good adsorbent should exhibit high stability and performance after multiple loading/regeneration cycles (Gnanasekaran et al. 2017; Abdelhameed et al. 2016; Saravanan et al. 2016). This feature was also considered in this essay by carrying out the following reusability tests: 85 mg of Cu–BTC was dispersed in 200 mL of water containing 75 ppm of ^{14}C-ethion insecticide and then stirred for 150 min at 25 °C and pH 7. After each run, the Cu–BTC was washed with acetonitrile (ethion dissolves well in acetonitrile) and dried in oven at 80 °C for 2 h, in order to be used in a next cycle under the same experimental conditions.

Removal ability of Cu-BTC decreases from 95.5 to 82.1% after six cycles (Fig. 9). Small adsorption reduction of 3.5% is observed after the first regeneration, increasing to 14% in the sixth cycle. This indicates that Cu–BTC may be successfully desorbed using a simple organic solvent. These results evidence that Cu–BTC is stable and highly effective for the removal of organophosphorus insecticide ethion from wastewater.

Table 2 Comparison of ethion and malathion insecticides removal using different adsorbents

Adsorbents	Adsorption capacity (mg g^{-1})	References
Bagasse fly ash	0.002	Gupta et al. (2002)
Thermally treated egg shell material	0.318	Elwakeel and Yousif (2010)
Multiwalled carbon nanotubes	20	Dehghani et al. (2017)
Aminated poly(glycidyl methacrylate)	66.83	Younis et al. (2017)
Activated carbon from agricultural wastes	32.1	Habila et al. (2015)
Rice husk	4.29	Kumar et al. (2014)
Activated rice husk	16.13	Kumar et al. (2014)
Commercially available powdered activated carbon	21.74	Kumar et al. (2014)
De-Acidite FF-IP resin	3.5	Naushad et al. (2013)
Cu-BTC@cotton composite	182	Abdelhameed et al. (2016)
Cu-BTC for removal of ethion	122	Current work

Mechanism of adsorption

Six different types of mechanisms were proposed for the interaction between adsorbates and MOFs active sites (Khan et al. 2013; Hasan and Jhung 2015): (1) complex formation; (2) acid–base interaction; (3) π–π interactions; (4) hydrogen bonding; (5) electrostatic interaction; and (6) adsorption based on hydrophobic interactions. Considering

that the ^{14}C-ethion insecticide contains functional groups such as P–O, with lone electrons, and that Cu-BTC presents open (unsaturated) metal coordination sites, it is proposed that, upon adsorption, ^{14}C-ethion binds Cu(II). Support for this mechanism comes from FTIR (Fig. 3): ethion P-OEt bands at 816 and 796 cm^{-1} disappear upon insecticide adsorption indicating coordination to copper(II) via the phosphoryl (P–O) group. Cu-BTC contains channels ca. 0.9 nm (Vishnyakov et al. 2003) across, while the ethion molecule measures ca. 0.7 nm from oxygen to oxygen on the two phosphoryl groups. If one considers also a typical Cu–O bond length of ca. 0.18 nm (Bae et al. 2011), it is clear that the ethion molecule can easily bridge two Cu(II) atoms across the MOF channel. Therefore, this mechanism seems an important contribution to the uptake of ^{14}C-ethion by Cu-BTC.

Comparison of Cu-BTC performance with other materials

Table 2 compares the results obtained in this work and in other essays targeting the removal of ethion and malathion (insecticides with similar structure) from aqueous solutions. Among the several materials, such as residues, activated carbons, carbon nanotubes, resins, Cu-BTC MOF and Cu-BTC@cotton composite, listed Cu-BTC materials exhibit the best results. In fact, their adsorption capacities of 122 and 182 mg g^{-1}, respectively, largely surpass the affinities of the remaining materials, suggesting that Cu-BTC is a promising material for the removal of insecticides from aqueous solutions.

Conclusion

Cu-BTC was successfully used as adsorbent for the efficient removal of ^{14}C-ethion insecticide from wastewater. The optimized values of ethion concentration, contact time, pH, temperature and Cu-BTC dose were found to be 75 mg L^{-1}, 150 min, pH 7, 25 °C and 0.425 g L^{-1}, respectively. Cu-BTC showed an adsorption capacity ca. 122 mg g^{-1}, removing 94% of ^{14}C-ethion from aqueous solution. Concerning equilibrium, the system exhibits the unusual BET trend of type IV. Brunauer–Deming–Deming–Teller and Zhu–Gu isotherms achieved excellent results, with only 1.99 and 3.95% of error, respectively. A pseudo-first-order model was able to represent reliably the adsorption kinetics of the pesticide removal along time, and it was shown that under the studied operating conditions this equation is equivalent to the linear driving force model of Glueckauf. FTIR and simple pore size considerations confirm that the ethion adsorption occurs via coordination of the phosphoryl groups to copper(II). Reusability tests showed that Cu-BTC was stable and maintained good adsorption performance over six cycles. In summary, MOFs are promising materials for removing pesticides from wastewaters.

Acknowledgements The authors would like to thank the help of Prof. Dr. H. Kamel, Radioisotopes Department, Atomic Energy Authority, Cairo, Egypt, in the radioactivity measurements. This work was developed within the scope of the projects CICECO-Aveiro Institute of Materials (Ref. FCT UID/CTM/50011/2013) and UI QOPNA (Ref. FCT UID/QUI/00062/2013), financed by national funds through the FCT/MEC and when appropriate co-financed by FEDER under the PT2020 Partnership Agreement.

References

Abdel-Gawad H, Abdelhameed RM, Elmesalamy AM, Hegazi B (2011) Distribution and elimination of ^{14}C-ethion insecticide in chamomile flowers and oil. Phosphorus Sulfur Silicon 186:2122–2134. doi:10.1080/10426507.2011.588506

Abdelhameed RM, Abdel-Gawad H, Elshahat M, Emam HE (2016) Cu–BTC@cotton composite: design and removal of ethion insecticide from water. RSC Adv 6:42324–42333. doi:10.1039/C6RA04719J

Abdelhameed RM, Emam HE, Rocha J, Silva AMS (2017) Cu-BTC metal–organic framework natural fabrics composites for fuel purification. Fuel Process Technol 159:306–312. doi:10.1016/j.fuproc.2017.02.001

Ahmad T, Rafatullah M, Ghazali A, Sulaiman O, Hashim R, Ahmad A (2010) Removal of pesticides from water and wastewater by different adsorbents: a review. J Environ Sci Health Part C 28:231–271. doi:10.1080/10590501.2010.525782

Aniceto JPS, Silva CM (2015) Preparative chromatography: batch and continuous. In: Anderson JL, Berthod A, Pino V, Stalcup A (eds) Analytical separation science, vol 5, Chapter 4. Wiley, New York, pp 1207–1313

Asfaram A, Ghaedi M, Agarwal S (2015) Removal of basic dye Auramine-O by ZnS:Cu nanoparticles loaded on activated carbon: optimization of parameters using response surface. RSC Adv 5:18438–18450. doi:10.1039/C4RA15637D

Bae G-T, Dellinger B, Hall RW (2011) Density functional calculation of the structure and electronic properties of CunOn (n = 1–8) clusters. J Phys Chem A 115:2087–2095. doi:10.1021/jp104177q

Brunauer S, Deming LS, Deming WE, Teller E (1940) On a theory of the van der waals adsorption of gases. J Am Chem Soc 62:1723–1732. doi:10.1021/ja01864a025

Danmaliki GI, Saleh TA (2017) Effects of bimetallic Ce/Fe nanoparticles on the desulfurization of thiophenes using activated carbon. Chem Eng J 307:914–927. doi:10.1016/j.cej.2016.08.143

Danmaliki GI, Saleh TA, Shamsuddeen AA (2017) Response surface methodology optimization of adsorptive desulfurization on nickel/activated carbon. Chem Eng J 313:993–1003. doi:10.1016/j.cej.2016.10.141

Dehghani MH, Niasar ZS, Mehrnia MR, Shayeghi M, Al-Ghouti MA, Heibati B, McKay G, Yetilmezsoy K (2017) Optimizing the removal of organophosphorus pesticide malathion from water using multi-walled carbon nanotubes. Chem Eng J 310:22–32. doi:10.1016/j.cej.2016.10.057

Do DD (1998) Adsorption analysis: equilibrium kinetics. Imperial College Press, London

Ebadi A, Mohammadzadeh JSS, Khudiev A (2009) What is the correct form of BET isotherm for modeling liquid phase

adsorption? Adsorption 15:65–73. doi:10.1007/s10450-009-9151-3
Elwakeel KZ, Yousif AM (2010) Adsorption of malathion on thermally treated egg shell material. Water Sci Technol 61:1035–1041. doi:10.2166/wst.2010.005
Foster LJR, Kwan BH, Vancov T (2004) Microbial degradation of the organophosphate pesticide, Ethion. FEMS Microbiol Lett 240(1):49–53. doi:10.1016/j.femsle.2004.09.010
Girods P, Dufour A, Fierro V, Rogaume Y, Rogaume C, Zoulalian A, Celzard A (2009) Activated carbons prepared from wood particleboard wastes: characterization and phenol adsorption capacities. J Hazard Mater 166:491–501. doi:10.1016/j.jhazmat.2008.11.047
Glueckauf E (1955) Theory of chromatography—Part X. Formulae for diffusion into spheres and their application to chromatography. Trans Faraday Soc 51:1540–1551. doi:10.1039/TF9555101540
Glueckauf E, Coates J (1947) Theory of chromatography—part IV. The influence of incomplete equilibrium on the front boundary of chromatograms and on the effectiveness of separation. J Chem Soc 1315–1321. doi:10.1039/JR9470001315
Gnanasekaran L, Hemamalini R, Saravanan R, Ravichandran K, Gracia F, Agarwal S, Gupta VK (2017) Synthesis and characterization of metal oxides (CeO_2, CuO, NiO, Mn_3O_4, SnO2 and ZnO) nanoparticles as photocatalysts for degradation of textile dyes. J Photochem Photobiol B Biol 173:43–49. doi:10.1016/j.jphotobiol.2017.05.027
Gupta VK, Jain C, Ali I, Chandra S, Agarwal S (2002) Removal of lindane and malathion from wastewater using bagasse fly ash—a sugar industry waste. Water Res 36:2483–2490. doi:10.1016/S0043-1354(01)00474-2
Gupta VK, Tyagi I, Agarwal S, Sadegh H, Shahryari-ghoshekandi R, Yari M, Yousefi-Nejat O (2015) Experimental study of surfaces of hydrogel polymers HEMA, HEMA–EEMA–MA, and PVA as adsorbent for removal of azo dyes from liquid phase. J Mol Liq 206:129–136. doi:10.1016/j.molliq.2015.02.015
Gupta VK, Saravanan R, Agarwal S, Gracia F, Khan MM, Qin J, Mangalaraja RV (2017) Degradation of azo dyes under different wavelengths of UV light with chitosan–SnO_2 nanocomposites. J Mol Liq 232:423–430. doi:10.1016/j.molliq.2017.02.095
Habila MA, Alothman ZA, Al-Tamrah SA, Ghafar AA, Soylak M (2015) Activated carbon from waste as an efficient adsorbent for malathion for detection and removal purposes. J Ind Eng Chem 32:336–344. doi:10.1016/j.jiec.2015.09.009
Hasan Z, Jhung SH (2015) Removal of hazardous organics from water using metal–organic frameworks (MOFs): plausible mechanisms for selective adsorptions. J Hazardous Mater 283:329–339. doi:10.1016/j.jhazmat.2014.09.046
Ho Y-S, McKay G (1999) Pseudo-second order model for sorption processes. Process Biochem 34:451–465. doi:10.1016/S0032-9592(98)00112-5
Hoffmann I, Oppel C, Gernert U, Barreleiro P, Von Rybinski W, Gradzielski M (2012) Adsorption isotherms of cellulose-based polymers onto cotton fibers determined by means of a direct method of fluorescence spectroscopy. Langmuir 28:7695–7703. doi:10.1021/la300192q
Huang MR, Peng QY, Li XG (2006) Rapid and effective adsorption of lead ions on fine poly(phenylenediamine) microparticles. Chem Eur J 12:4341–4350. doi:10.1002/chem.200501070
Khan NA, Hasan Z, Jhung SH (2013) Adsorptive removal of hazardous materials using metal–organic frameworks (MOFs): a review. J Hazard Mater 244:444–456. doi:10.1016/j.jhazmat.2012.11.011
Kumar P, Singh H, Kapur M, Mondal MK (2014) Comparative study of malathion removal from aqueous solution by agricultural and commercial adsorbents. J Water Process Eng 3:67–73. doi:10.1016/j.jwpe.2014.05.010
Largergren S (1898) Zur theorie der sogenannten adsorption geloster stoffe. Kungliga svenska vetenskapsakademiens. Handlingar 24:1–39
Li H, Eddaoudi M, O'Keeffe M, Yaghi OM (1999) Design and synthesis of an exceptionally stable and highly porous metal–organic framework. Nature 402:276–279. doi:10.1038/46248
Liu J, Culp JT, Natesakhawat S, Bockrath BC, Zande B, Sankar S, Garberoglio G, Johnson JK (2007) Experimental and theoretical studies of gas adsorption in $Cu_3(BTC)_2$: an effective activation procedure. J Phys Chem C 111:9305–9313. doi:10.1021/jp071449i
Naushad M, Alothman Z, Khan M (2013) Removal of malathion from aqueous solution using De-Acidite FF-IP resin and determination by UPLC–MS/MS: equilibrium, kinetics and thermodynamics studies. Talanta 115:15–23. doi:10.1016/j.talanta.2013.04.015
Nile Basin Initiative—Nile basin national water quality monitoring baseline study report for Egypt (2005) Nile Basin Regional Water Quality Monitoring Baseline Study Report—Final
Qadir M, Mateo-Sagasta J, Jiménez B, Siebe C, Siemens J, Hanjra MA (2015) Environmental risks and cost-effective risk management in wastewater use systems. In: Drechsel P, Qadir M, Wichelns D (eds) Wastewater—economic asset in an urbanizing world. Springer, Netherlands, pp 55–72
Robati D, Mirza B, Rajabi M, Moradi O, Tyagi I, Agarwal S, Gupta VK (2016) Removal of hazardous dyes-BR 12 and methyl orange using graphene oxide as an adsorbent from aqueous phase. Chem Eng J 284:687–697. doi:10.1016/j.cej.2015.08.131
Rodrigues AE, Silva CM (2016) What's wrong with Lagergreen pseudo first order model for adsorption kinetics? Chem Eng J 306:1138–1142. doi:10.1016/j.cej.2016.08.055
Rowsell JL, Yaghi OM (2006) Effects of functionalization, catenation, and variation of the metal oxide and organic linking units on the low-pressure hydrogen adsorption properties of metal–organic frameworks. J Am Chem Soc 128:1304–1315. doi:10.1021/ja056639q
Sainio T, Turku I (2010) Adsorption of cationic surfactants on a neutral polymer adsorbent: investigation of the interactions by using mathematical modeling. Coll Surf A 358:57–67. doi:10.1016/j.colsurfa.2010.01.031
Saleh TA, Sarı A, Tuzen M (2017) Effective adsorption of antimony(III) from aqueous solutions by polyamide-graphene composite as a novel adsorbent. Chem Engin J 307:230–238. doi:10.1016/j.cej.2016.08.070
Saravanan R, Sacari E, Gracia F, Khan MM, Mosquera E, Gupta VK (2016) Conducting PANI stimulated ZnO system for visible light photocatalytic degradation of coloured dyes. J Mol Liq 221:1029–1033. doi:10.1016/j.molliq.2016.06.074
Stavila V, Talin A, Allendorf M (2014) MOF-based electronic and opto-electronic devices. Chem Soc Rev 43:5994–6010. doi:10.1039/c4cs00096j
Tanner PA, Leung K-H (1996) Spectral interpretation and qualitative analysis of organophosphorus pesticides using ft-raman and ft-infrared spectroscopy. Appl Spectrosc 50:565–571
Vishnyakov A, Ravikovitch PI, Neimark AV, Bülow M, Wang QM (2003) Nanopore structure and sorption properties of Cu–BTC metal–organic framework. Nano Lett 3:713–718. doi:10.1021/nl0341281
Younis SA, Ghobashy MM, Samy M (2017) Development of aminated poly(glycidyl methacrylate) nanosorbent by green gamma radiation for phenol and malathion contaminated wastewater treatment. J Environ Chem Eng 5:2325–2336. doi:10.1016/j.jece.2017.04.024

Zhang T, Lin W (2014) Metal–organic frameworks for artificial photosynthesis and photocatalysis. Chem Soc Rev 43:5982–5993. doi:10.1039/C4CS00103F

Zhu B-Y, Gu T (1989) General isotherm equation for adsorption of surfactants at solid/liquid interfaces. Part 1. Theoretical. J Chem Soc Faraday Trans 1(85):3813–3817. doi:10.1039/F19898503813

Zhu B-Y, Gu T, Zhao X (1989) General isotherm equation for adsorption of surfactants at solid/liquid interfaces. Part 2. Applications. J Chem Soc Faraday Trans 1(85):3819–3824. doi:10.1039/F19898503819

Zhu X, Li B, Yang J, Li Y, Zhao W, Shi J, Gu J (2014) Effective adsorption and enhanced removal of organophosphorus pesticides from aqueous solution by Zr-based MOFs of UIO-67. ACS Appl Mater Interfaces 7:223–231. doi:10.1021/am5059074